AA Technical Memorandum ERL ETL-239

A CALIBRATION FOR MEASURING C_n^2 WITH THE NOAA/ETL/AL 915-MHZ RADAR

A. B. White
R. G. Strauch
C. W. Fairall

Environmental Technology Laboratory
Boulder, Colorado
April 1994

noaa NATIONAL OCEANIC AND ATMOSPHERIC ADMINISTRATION / Environmental Research Laboratories

NOAA Technical Memorandum ERL ETL-239

A CALIBRATION FOR MEASURING C_n^2 WITH THE NOAA/ETL/AL 915-MHZ RADAR

A. B. White
R. G. Strauch
Cooperative Institute for Research in Environmental Sciences
University of Colorado
Boulder, Colorado

C. W. Fairall
Environmental Technology Laboratory

Environmental Technology Laboratory
Boulder, Colorado
April 1994

UNITED STATES DEPARTMENT OF COMMERCE

Ronald H. Brown
Secretary

NATIONAL OCEANIC AND ATMOSPHERIC ADMINISTRATION

D. James Baker
Under Secretary for Oceans and Atmosphere/Administrator

Environmental Research Laboratories

Alan R. Thomas
Director

NOTICE

Mention of a commercial company or product does not constitute an endorsement by NOAA/ERL. Use of information from this publication concerning proprietary products or the tests of such products for publicity or advertising purposes is not authorized.

For sale by the National Technical Information Service, 5285 Port Royal Road
Springfield, VA 22161

CONTENTS

A CALIBRATION FOR MEASURING C_n^2 WITH THE NOAA/ETL/AL 915-MHZ RADAR

A. B. White and R. G. Strauch
Cooperative Institute for Research in Environmental Sciences
University of Colorado
Boulder, Colorado

C. W. Fairall
NOAA/ERL Environmental Technology Laboratory
Boulder, Colorado

ABSTRACT. A time series of radar reflectivity was compared to a time series of the refractive index structure constant measured with a sonic anemometer and an infrared hygrometer mounted on a tower. This comparison was used to obtain a calibration for radar measurements of the refractive index structure constant. As another means of calibrating the radar, the response of the radar from the receiver input port through the various stages of signal processing was measured with a noise source. This information was also used to calibrate radar reflectivity measurements.

1. INTRODUCTION

During the months of July and August (1993), NOAA/ETL operated a NOAA/ETL/AL 915-MHz Radar (hereafter referred to as radar) at the Boulder Atmospheric Observatory (BAO) in Erie, Colorado. The purpose of this deployment was to obtain a calibration factor for calculating the refractive index structure function, C_n^2, from the backscattered signals received by the radar. To accomplish this task, the BAO tower was instrumented with an ATI sonic anemometer/thermometer and an Ophir fast infrared hygrometer at the 250-m level. We could not make use of the 300-m tower level for our deployment because this level was occupied by other instruments that would have interfered with the operation of the sonic anemometer/thermometer. Tower measurements of C_n^2 were then compared to radar signal-to-noise ratio (*SNR*) measurements. Using the reflectivity equation of Vanzandt et al. (1978), a radar system efficiency was calculated.

In a separate calibration experiment, a noise signal of known power was injected into the radar at the input to the receiver. The resulting output signal power from the radar control program was then recorded. This information was used to calibrate the radar receiver and the various stages of the Doppler signal processing. Using the standard radar equation in terms of received power (e.g., Gossard and Strauch, 1983), a radar system efficiency was calculated and compared to the *SNR*-based estimate. Both coded and uncoded pulse methods were examined.

2. TOWER C_n^2 MEASUREMENTS

The ATI sonic anemometer was operated to measure fluctuations in temperature, T', and the three-dimensional wind field (u', v', and w') at a rate of 10 Hz. Coincident measurements of fluctuating absolute humidity, Q', were made by the Ophir hygrometer at 20 Hz and pair-averaged to 10 Hz. The signals from both instruments were acquired with a common PC-based data system. Means, variances, and covariances were calculated for each 15-min data segment. In addition, the program produced spectra and cospectra using an 8192-point FFT. The time series was tapered with a Hamming window prior to computing the FFT to reduce truncation error. The 15-min statistics and spectral data were recorded in hourly files on magnetic tape. The 10-Hz data were not saved.

The T' and Q' data were used to calculate C_n^2 using two related, but slightly different, methods. We start by noting that it is convenient to use refractivity, N, instead of refractive index, n, where

$$N \equiv (n - 1) \times 10^6 \ . \tag{1}$$

For Q in units of g m^{-3} and T in K, N is given by

$$N = \frac{77.6\,P}{T}\left(1 + \frac{7733\,QR}{P}\right), \tag{2}$$

where $R = 2.87 \times 10^{-3}$ mb $m^3 \cdot g^{-1}$ K^{-1} is the gas constant for air, and P is the total pressure in millibars. Equation (2) follows from Doviak and Zrnic (1984), except that N has been rewritten in terms of absolute humidity, rather than vapor pressure.

For the first approach, we decompose each of the variables N, T, Q, and P into a mean, denoted by an overbar, and a fluctuating part, denoted by a prime, such that

$$N = \bar{N} + N' \tag{3a}$$

$$T = \bar{T} + T' \tag{3b}$$

$$Q = \bar{Q} + Q' \tag{3c}$$

$$P = \bar{P} + P' . \tag{3d}$$

In this analysis, pressure fluctuations can be ignored (Burk, 1980). After substituting these expressions in (2), we arrive at an equation for the fluctuating refractivity:

$$N' = -\left(\frac{77.6\,P + 1722\,\bar{Q}}{\bar{T}^2}\right)T' + \left(\frac{1722}{\bar{T}}\right)Q' \,. \tag{4}$$

The 10-Hz data and 15-min averages were used in (4) to calculate N' with P = 827 mb. Spectra of N' were also produced using an 8192-point FFT.

In the inertial subrange of isotropic turbulence, the structure function for fluctuations in x, C_x^2, is related to the one-dimensional variance spectral density, $S_x(k)$ (Panofsky and Dutton, 1984), by

$$S_x(k) = 0.25\,C_x^2\,k^{-5/3}\,, \tag{5}$$

where k is the spectral wavenumber. In (5), x could be N, T, or Q. Our spectral data were computed in frequency space with the product $fS_x(f)$ given as a function of frequency, f. We can easily switch from a wavenumber dependence to a frequency dependence using the transform $f = 2\pi\,k/\bar{u}$, where $\bar{u}$ is the mean horizontal wind measured by the sonic anemometer. After rearranging (5), we obtain

$$C_x^2 = 4\left(\frac{2\pi}{\bar{u}}\right)^{2/3} S_x(f)\,f^{5/3}\,. \tag{6}$$

We examined many spectra to find the spectral frequency range for which $S_N(f)$ most often exhibited the -5/3 power law characteristic of the inertial subrange. We chose to use the median spectral density in this range (0.1-0.5 Hz) for our analysis. To convert from C_N^2 to C_n^2, we simply multiply C_N^2 by 10^{-12}. We will refer to the tower values of C_n^2 using this method as $(C_n^2)_{T1}$,

$$(C_n^2)_{T1} = 4\times 10^{-12}\left(\frac{2\pi}{\bar{u}}\right)^{2/3} S_N(f)\,f^{5/3}\,. \tag{7}$$

In the second approach, we used the structure functions for temperature, C_T^2, and humidity, C_Q^2, calculated with (5) to infer C_n^2. We will refer to the tower values of C_n^2 using this method as $(C_n^2)_{T2}$. The dependence of C_n^2 on C_T^2 and C_Q^2 is found by taking the square of (4),

$$(C_n^2)_{T2} = a^2 C_T^2 - 2ab\, C_{TQ} + b^2 C_Q^2 , \tag{8a}$$

where

$$a = -77.6 \frac{P}{\bar{T}^2} - 1722 \frac{\bar{Q}}{\bar{T}^2} , \tag{8b}$$

and

$$b = \frac{1722}{\bar{T}} . \tag{8c}$$

This method requires us to estimate the structure functions for temperature and humidity as well as the structure function for temperature-humidity correlation, C_{TQ}, using the spectral data. We found, in particular, difficulty in estimating C_{TQ}. However, we can use the fact that the magnitude of the temperature-humidity correlation coefficient, r_{TQ}, given by

$$r_{TQ} = \frac{C_{TQ}}{\sqrt{C_T^2 C_Q^2}} , \tag{9}$$

cannot exceed unity to judge whether or not we obtained a good estimate of C_{TQ} from the TQ copsectrum. All data that violated this criterion were eliminated before computing $(C_n^2)_{T2}$.

The first method described has the advantage of requiring only one structure function estimate. Unfortunately, after the experiment, we discovered two coding errors in the section of the data acquisition program used to calculate N'. Specifically, errors made to both of the coefficients in (4) resulted in overestimating the temperature contribution and underestimating the humidity contribution each by roughly a factor of two. Because the 10-Hz data were not saved, we could not recompute the N-spectra. Figure 1 shows a scatterplot of C_n^2 determined by the two methods. The approximately 6-dB bias is caused by errors in the $(C_n^2)_{T1}$ calculation. Still, the correlation between the two methods is quite good; the correlation coefficient is 0.99. Because the magnitude of the error was consistent over the range of observed values, we used the average ratio between $(C_n^2)_{T1}$ and $(C_n^2)_{T2}$ to correct the $(C_n^2)_{T1}$ data.

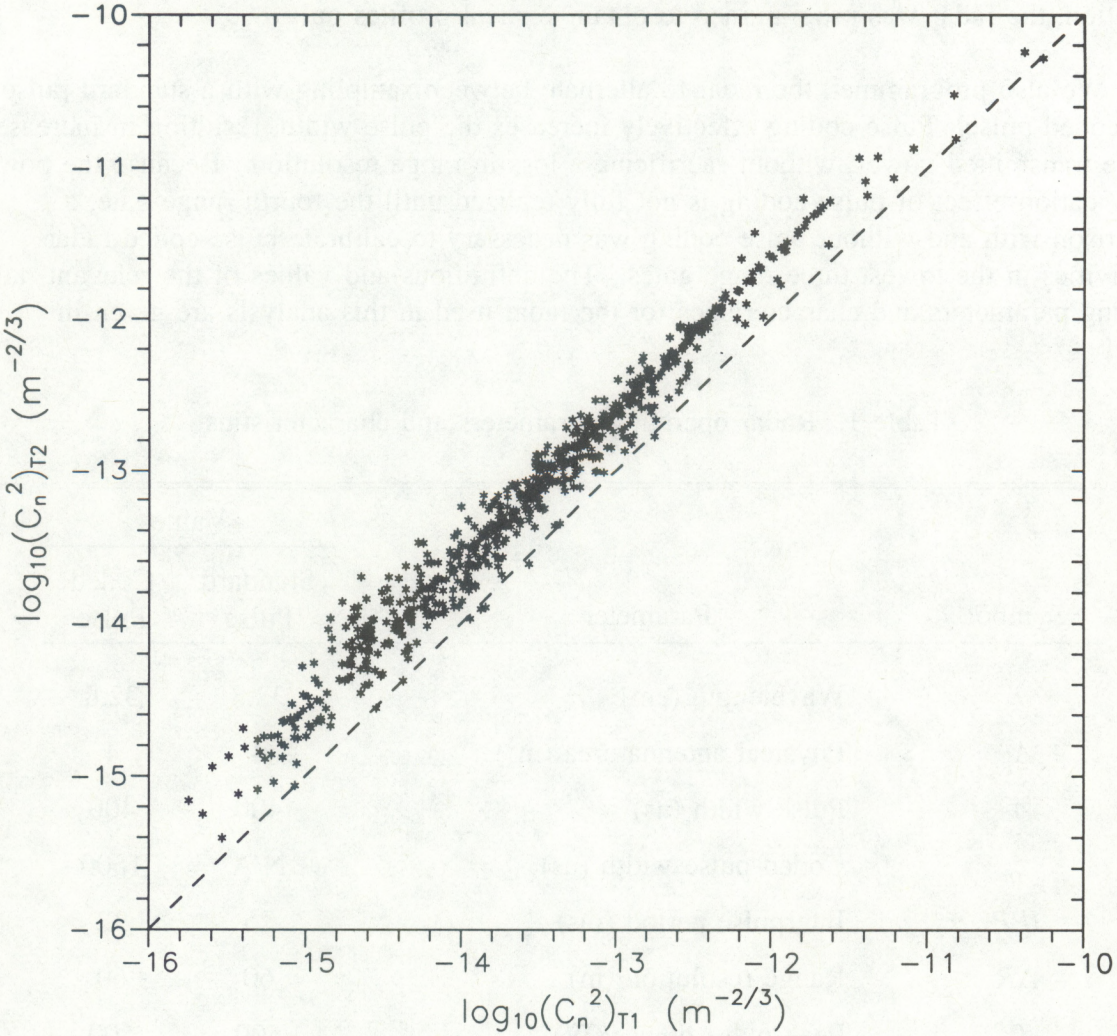

Figure 1. Scatterplot comparing tower C_n^2 data calculated using the two methods described in the text. The correlation coefficient is 0.99. The bias is caused by errors in the $(C_n^2)_{T1}$ calculation.

3. RADAR REFLECTIVITY MEASUREMENTS

The radar deployed at the BAO is a special seagoing version of the boundary-layer profiler developed at the NOAA Aeronomy Laboratory (Ecklund et al., 1988). The system uses a single flatplate, microstrip, phased-array antenna. For wind profiling, three beams are produced by electronically changing the phasing. However, for the purposes of this calibration, the radar was programmed to obtain vertical profiles only.

We also programmed the radar to alternate between sampling with a standard pulse and a coded pulse. Pulse coding effectively increases the pulse width, resulting in increased average transmitted power, without sacrificing a loss in range resolution. Because the power intensification effect of pulse coding is not fully realized until the fourth range gate, a comparison with and without pulse coding was necessary to calibrate pulse-coded radar reflectivities in the lowest three range gates. The definitions and values of the relevant radar operating parameters and characteristics for the radar used in this analysis are given in Table 1.

Table 1. Radar operating parameters and characteristics

Symbol	Parameter	Value	
		Standard Pulse	Coded Pulse
λ	Wavelength (cm)	32.8	32.8
A_p	Physical antenna area (m^2)	4	4
τ	Pulse width (ns)	400	400
τ_p	Coded pulse width (ns)	N/A	1600
IPP	Interpulse period (ms)	25	32
ΔR	Range resolution (m)	60	60
P_t	Peak pulse power (W)	500	500
n_c	Number of coherent integrations	320	250
T_{rx}	Receiver noise temperature (K)	450	450
T_s	Sky noise temperature (K)	30	30
ϕ	Beam elevation angle (deg)	90	90

In clear air, transmitted pulses from the radar scatter from refractive index inhomogeneities. The radar reflectivity, or scattering cross section per unit volume, η, is a measure of the scattering intensity. If we assume that the radar half-wavelength lies within the inertial subrange of turbulence, then

$$C_n^2 = \frac{\eta}{0.38} \lambda^{1/3} . \tag{10}$$

The problem then is to relate η to quantities that are directly measurable by the radar. The more common approach is to calibrate the signal power, P_s. However, this technique is based on a receiver calibration that depends on the radar operating parameters in use at the time of the calibration. A different approach that relates *SNR* to η avoids this problem by not requiring a separate receiver calibration. We will use both methods in our analysis. We first look at the *SNR* approach.

The scattered signals received by the radar are converted into Doppler spectra from which the *SNR* is estimated. Because of the complex nature of the Doppler signal processing, a special radar equation is needed to relate η to *SNR*. We use the Doppler radar reflectivity equation given by VanZandt et al. (1978):

$$\eta = \frac{9\pi\, ck\left(\alpha T_s + T_{rx}\right) R^2 SNR}{2\alpha^2 P_t A_e n_c (\Delta R)^2 \sin(\phi)} , \tag{11}$$

where $c = 2.998 \times 10^8$ m s^{-1} is the speed of light, $k = 1.3803 \times 10^{-23}$ J mol^{-1} K^{-1} is Boltzmann's constant, and α is the radar "system" efficiency. This parameter accounts for absorptive and radiative losses in the transmission line and antenna. All other variables are defined in Table 1. The effective antenna area, A_e, is related to the physical antenna area, A_p, by the antenna efficiency. This relationship is well-known for parabolic antennas, but has not yet been determined for the flat, rectangular, phased-array antenna design. Because A_e is unknown, we will let α include a factor for the antenna efficiency and use A_p in place of A_e.

In (11), noise contributions from internal (electronic) and external (sky) noise sources are expressed as noise temperatures. At 915 MHz, the geometric-mean galactic temperature for an elevation angle of 90° is about 30 K (Doviak and Zrnic, 1984). Because $\alpha < 1$, and given the values in Table 1, we expect $\alpha T_s << T_{rx}$. Therefore, we will neglect sky noise in our calculations.

We can eliminate R^2 in (11) by introducing a new variable, *RCSNR* (range-corrected signal-to-noise ratio), where $RCSNR = R^2 SNR$. Upon combining (10) with (11) and after rearranging, we get

$$(C_n^2)_{SNR} = 1.54 \times 10^{-13} \left[\frac{T_{rx} \lambda^{1/3} RCSNR}{\alpha^2 P_t A_p n_c (\Delta R)^2 \sin(\phi)} \right] \tag{12}$$

The subscript "*SNR*" is used here to denote a general radar C_n^2 equation based on radar *SNR* measurements. The specific characteristics of individual radars are expressed by the variables in the brackets.

Note that in (12), the radar system noise power at the receiver input is known (or measured) so that calibrated values of C_n^2 can be obtained from *SNR* measurements. The value of signal power, P_s, obtained from the output of the signal processor is simply a relative number such that $P_s = (SNR) \times$ (noise level at the output of the signal processor). No calibration of the radar receiver is required because noise and signal undergo the same processing steps. On the other hand, if we calibrate P_s in terms of received power, P_r, then we can use another form of the radar equation to obtain a C_n^2 calibration.

Received power was calibrated in the following way. Using a noise diode, a broad-band signal of known power was injected at the input to the receiver. A broad-band signal was used instead of a sinusoid because of the difficulty associated with producing a sinusoidal test signal locked to the radar with constant Doppler shift and known power. This input signal was then processed by the radar control program in the same way that backscattered signals from the atmosphere are processed. The signal power from the resulting averaged spectrum was compared to the power of the original input signal to determine the gain associated with the receiver and the signal processing. The input signal was varied to obtain a calibration curve. The results are shown in Fig. 2.

The standard radar equation, in terms of received power, is given by Gossard and Strauch (1983),

$$P_r = \pi \alpha^2 P_t A_p \sin(\phi) \frac{\Delta R \eta}{128 \ln(2) R^2} , \qquad (13)$$

where again we have replaced A_e with A_p and allowed α to account for the antenna efficiency, as well as the absorptive and radiative losses in the transmission line and antenna. As in (11), two factors of α (i.e., α^2) are necessary in (14) because P_t is measured at the output of the transmitter and P_r is calibrated at the input to the receiver.

If we introduce range-corrected received power (RCP_r) and combine (10) with (13), we arrive at an alternate equation for (12),

$$(C_n^2)_P = 74.32 \left(\frac{\lambda^{1/3} RCP_r}{\alpha^2 P_t A_p \Delta R \sin(\phi)} \right) \qquad (14)$$

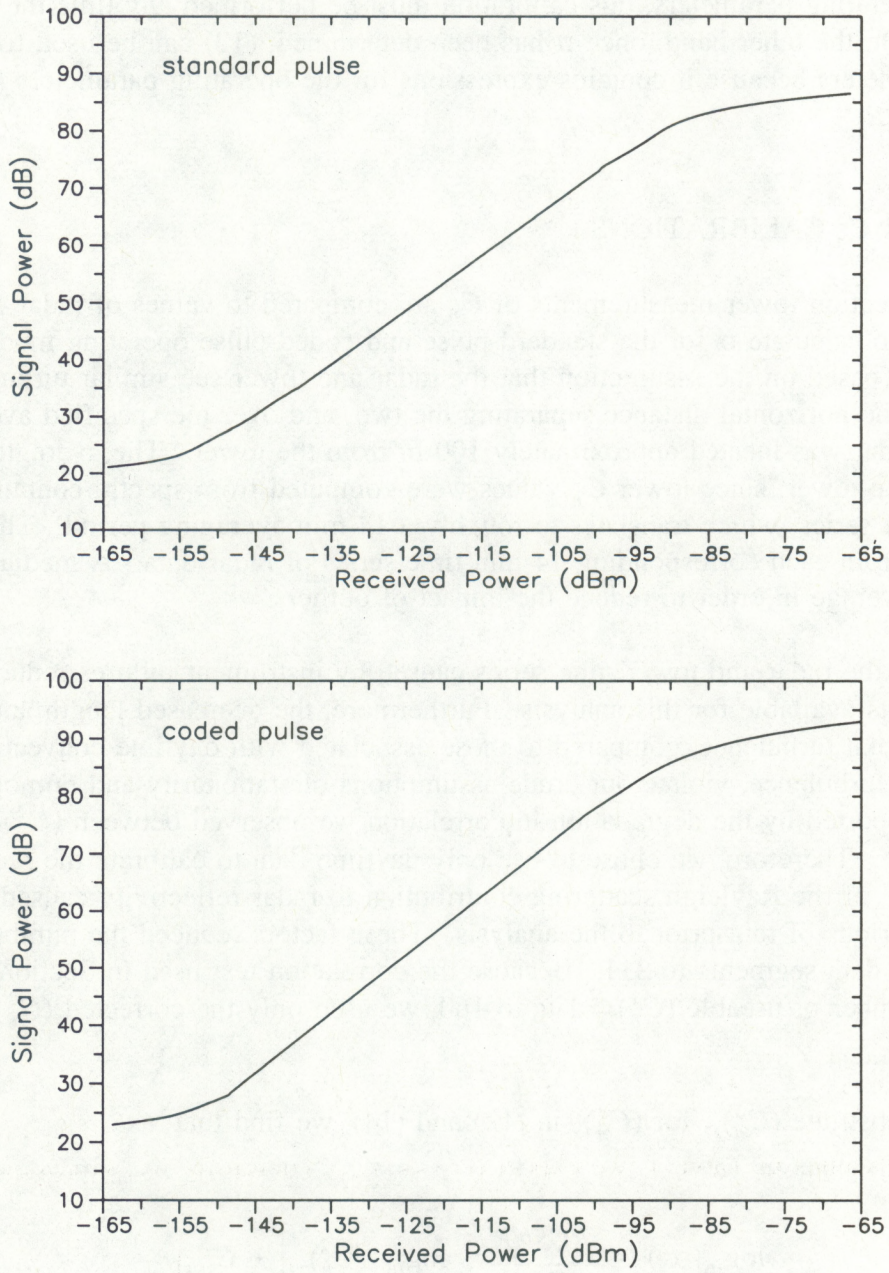

Figure 2. Received power calibration curves measured for the NOAA/ETL/AL 915-MHz radar with the operating parameters shown in Table 1.

The subscript "P" refers to a radar C_n^2 equation based on radar measurements of received power. At first appearance, (14) looks slightly easier to use than (12). However, remember that a receiver calibration is required to convert P_s to P_r. Because P_s depends on the values of the radar operating parameters, this calibration must be performed any time the parameters are changed. On the other hand, once α has been determined, (12) can be used for any set of operating parameters because it contains expressions for the operating parameters that effect the value of *SNR*.

4. RADAR C_n^2 CALIBRATIONS

In this section tower measurements of C_n^2 are compared to values of radar *RCSNR* and RCP_r in order to calculate α for the standard-pulse and coded-pulse operating modes. These calibrations are based on the assumption that the radar and tower see similar turbulence structure over the horizontal distance separating the two, and over the specified averaging period. The radar was located approximately 100 m from the tower. The averaging period is defined by the tower, since tower C_n^2 values were computed from spectra containing an 8192-point time series, which translates to roughly a 14-min averaging period. The median was extracted from each corresponding 14-min time series of radar data. A median was used instead of an average in order to reduce the impact of outliers.

Gaps in the radar and tower time series caused by instrument failures reduced the number of points available for this analysis. Furthermore, the decreased length and time scales of nocturnal turbulence, compared to those associated with daytime convective boundary layer turbulence, violate our crude assumptions of stationarity and homogeneity. This fact is supported by the degradation in correlation we observed between $(C_n^2)_{T1}$ and radar *RCSNR* at night. Therefore, we chose to use only daytime data to calibrate the radar for C_n^2. Finally, because of the Rayleigh scattering contribution to radar reflectivity caused by rain, we removed periods of rain prior to the analysis. These factors reduced the number of useable 14-min data segments to 311. Because the correlation test used in Section 2 further reduced the number of useable $(C_n^2)_{T2}$ data to 160, we used only the corrected $(C_n^2)_{T1}$ in our analysis.

If we substitute $(C_n^2)_{T1}$ for $(C_n^2)_R$ in (12) and (14), we find that

$$\log_{10}(\alpha^2) = \frac{RCSNR}{10} - \log_{10}\left[(C_n^2)_{T1}\right] + C_{SNR} \tag{15a}$$

$$\log_{10}(\alpha^2) = \frac{RCP_r}{10} - \log_{10}\left[(C_n^2)_{T1}\right] + C_P, \tag{15b}$$

where C_{SNR} and C_P take the place of all constants and radar operating parameters, and *RCSNR* and RCP_r are now in units of dB. Using the values given in Table 1, we find that for the standard-pulse mode, $C_{SNR} = -19.683$ and $C_P = -3.369$. For the coded-pulse mode, we include a factor of 4 to account for the increased length of the coded pulse to obtain $C_{SNR} = -20.178$ and $C_P = -3.972$. The differences given by the first two terms on the righthand side of (15a) and (15b) provide the calibration.

The radar data used in this analysis were obtained from the third radar range gate. For the radar operating in a pulse-coded mode, this presents a problem because the coding is not completed until the fourth range gate. As a result, the power transmitted in the lowest three range gates is reduced. A correction must be applied to these data if we are to obtain a calibration that is applicable to all pulse-coded range gates.

An additional factor that affects the signal power in the lowest few range gates of both the standard and pulse-coded operating modes is the receiver recovery from the blanking pulse. The receiver sensitivity must be sufficient to detect the signal amplitudes of the atmospheric signals, which contain only a small fraction of the power transmitted in the pulse. A blanking pulse is used to prevent receiver saturation caused by small amounts of leakage power from the transmitter. The number of gates that are affected by receiver recovery depends on the delay time between transmission and reception, which sets the height of the first gate.

Median profiles of radar *RCSNR* and RCP_r were produced for both the standard-pulse and coded-pulse modes. The results are shown in Fig. 3. From the standard-pulse profiles, it appears that only the first two range gates are influenced by the receiver recovery. To estimate this effect on these gates, we linearly extrapolated the part of the standard-pulse profiles between 278 m (gate 3) and 878 m (gate 13) down to 150 m. The difference between the extrapolation and the standard-pulse profile gives us the loss factors shown in Table 2. The same correction factors are applicable to the coded-pulse profiles because both operating modes used the same delay time.

The remaining difference between the coded-pulse profiles and the standard-pulse profiles is caused by partial pulse coding. The difference profiles for *RCSNR* and RCP_r are shown in Fig. 4. The average difference in range gates 5-20 was compared to the difference in the first three gates to determine the offsets. The results are reported in Table 2. The numbers in parentheses were calculated by Ghebrebrhan (1990) using a mathematical model. Aside from gate 2, the model and observations agree fairly well for the *SNR* profile. For gate 3, the gate of interest, the combined loss due to receiver recovery and partial decoding is -3.2 dB for *RCSNR* and -1.8 dB for RCP_r.

The appropriate loss factors from Table 2 were added to the radar data before comparing to the tower measurements. Then (15) was used to calculate the calibration constant or radar system efficiency. The results are shown in Table 3. Scatterplots

comparing the two independent estimates of C_n^2 are shown in Fig. 5. Much of the scatter may be caused by the fact that the tower measures a time-averaged C_n^2 over a very thin layer of the atmosphere, whereas the radar deduces a C_n^2 that is the combination of a time average over the radar sampling period, and a spatial average over the radar pulse volume. Because only one instrumented level was available on the tower, this difference in sampling could not be explored further.

Table 2. Loss factors for receiver recovery and partial decoding*

	SNR Loss Factors		Received Power Loss Factors	
Gate	Receiver Recovery	Partial Decoding	Receiver Recovery	Partial Decoding
1	-5.6	-9.6 (-10)	-15.5	-7.7
2	-0.6	-4.3 (-7.8)	-1.1	-5.7
3	**0.0**	**-3.2** (-3)	**0.0**	**-1.8**
4	0.0	+0.4 (0)	0.0	-2.2
5	0.0	-0.3 (0)	0.0	-1.6
6	0.0	-0.2 (0)	0.0	-1.2

*Values are in dB. Data highlighted in bold are for the radar range gate used in the calibration. The numbers in parentheses are from Ghebrebrhan (1990).

Table 3. NOAA/ETL/AL 915-MHz radar system efficiency*

	Coded Pulse		Standard Pulse	
	RCSNR	RCP_r	*RCSNR*	RCP_r
Log average	0.21	0.14	0.17	0.13
Median	0.22	0.14	0.17	0.14
Linear average	0.27	0.17	0.21	0.17

*Radar system efficiency is defined to include the antenna efficiency (see Section 3).

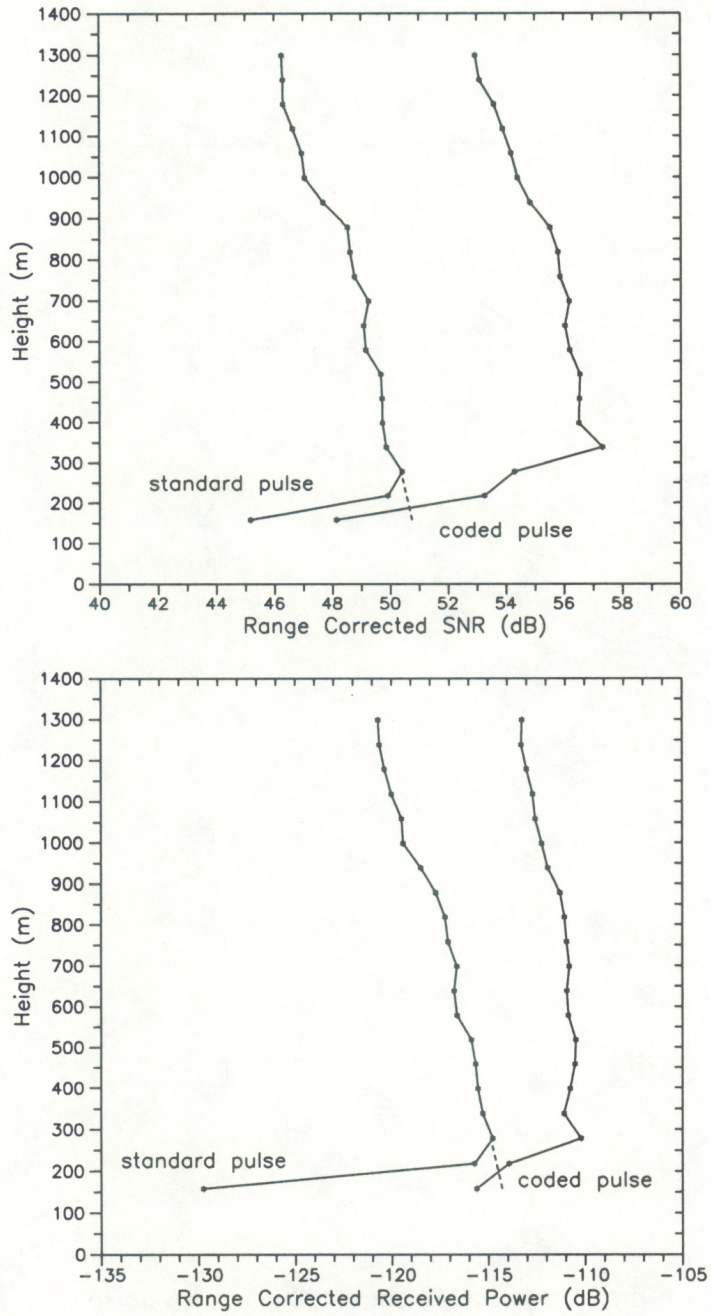

Figure 3. Median profiles of range-corrected signal-to-noise ratio and range-corrected received power measured with the NOAA/ETL/AL 915-MHz radar. The dashed lines near the bottom of the profiles show the extrapolations used to calculate the receiver recovery loss factor.

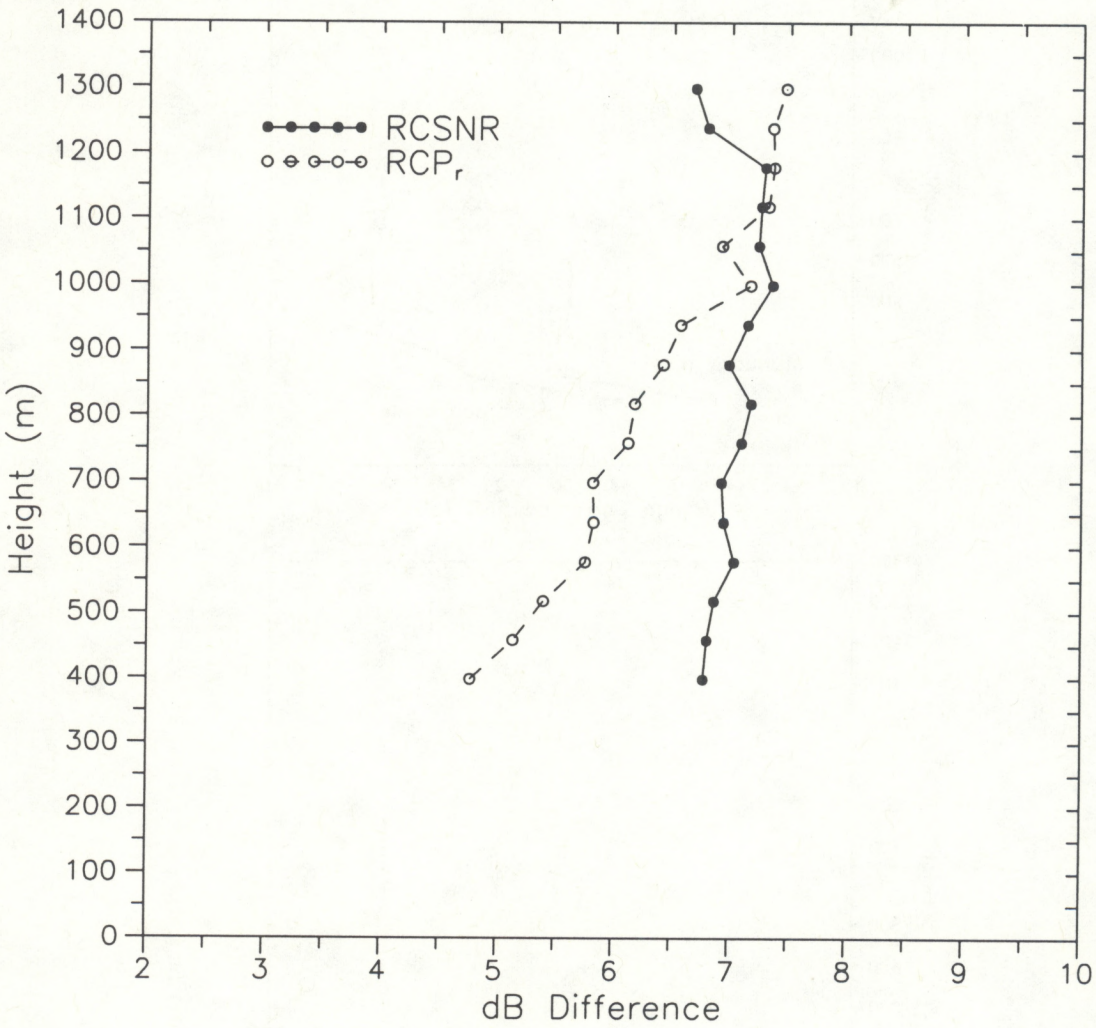

Figure 4. Difference profiles for range-corrected signal-to-noise ratio and range-corrected received power measured with the radar alternating between a coded pulse mode and an uncoded pulse mode. Data are shown for radar range gates 5-20.

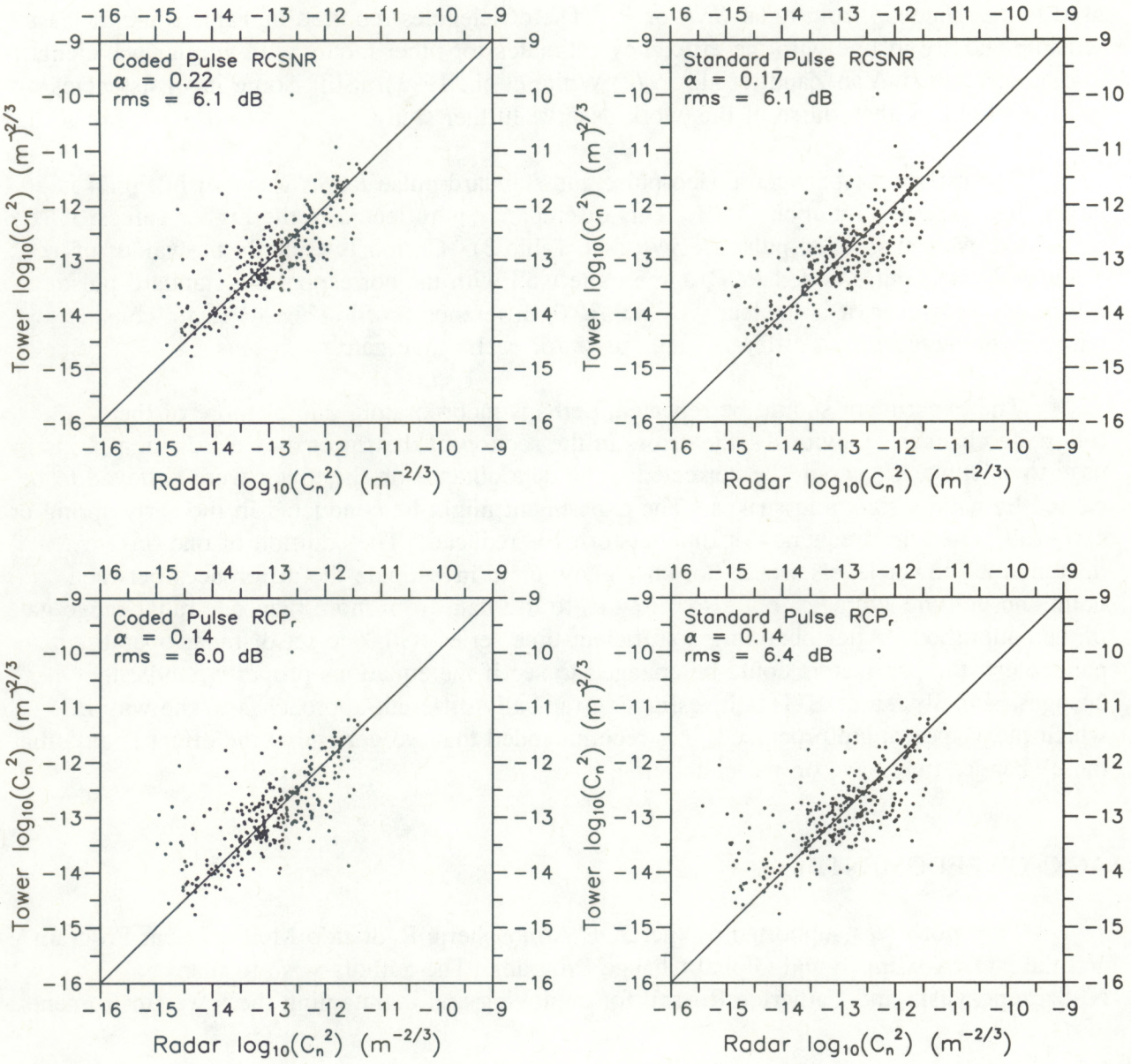

Figure 5. Scatterplots comparing C_n^2 measured on the tower with C_n^2 calculated from radar reflectivity. The radar variable, the calibration constant used for the radar calculation, and the rms error are shown in the upper left corner of each plot.

5. SUMMARY AND RECOMMENDATIONS

In this paper, we compared in situ measurements of C_n^2 made on a tower with remotely sensed measurements of radar reflectivity made by the NOAA/ETL 915-MHz radar. This comparison allowed us to estimate the radar system efficiency, which, in turn, can be used to calculate C_n^2 from radar *SNR* or P_r. The efficiencies reported in Table 3 are at least sensible and are in line with the efficiency estimates for other radars with similar wavelength-to-diameter ratios (Van Zandt et al., 1978; White et al., 1991). Still, some inconsistencies uncovered during the course of this work deserve further study.

The difference between coded-pulse and standard-pulse *RCSNR* shown in Fig. 4 is larger than expected by about 3 dB. This discrepancy is reflected in the higher values of α calculated using the coded-pulse *RCSNR* (see Table 3). Curiously enough, the values of α calculated using pulse-coded RCP_r agree quite well with the corresponding standard pulse estimates. However, it is unclear why the RCP_r difference profile (Fig. 4) is not constant with height, suggesting a different value of α for each range gate.

The experiment should be repeated, perhaps incorporating one or more of the following changes. Obviously, the errors in the section of the tower data acquisition program used to calculate C_n^2 should be corrected. The data outages on the tower were believed to be caused by nearby lightning strikes. The experiment might be conducted in the early spring or early fall, when the frequency of thunderstorms is reduced. The addition of one or two instrumented tower levels would not only allow us to investigate the differences between point and volume averages, but also allow us to use data from more than one radar range gate in the calibration. After obtaining a sufficient time series with one set of radar operating parameters, the parameters could be changed to see if the equations properly handle the changes. Finally, since ETL is investigating radically different approaches to the way in which radar spectra are processed, it is recommended that we determine the effect if any, that these changes may have on the calibration.

ACKNOWLEDGMENTS

This work was supported by the DOE Atmospheric Radiation Measurement Program and the NOAA Climate and Global Change Program. The authors wish to thank N. Szczepczynski and Catherine Russell for deploying and maintaining the tower instruments.

REFERENCES

Burk, S. D., 1980. Refractive index structure parameters: Time-dependent calculations using a numerical boundary-layer model. *J. Appl. Meteorol.* **19**:562-576.

Doviak, R. J., and D. S. Zrnic, 1984. *Doppler Radar and Weather Observations*. Academic Press, Orlando, 458 pp.

Ecklund, W. L., D. A. Carter, and B. B. Balsley, 1988. A UHF wind profiler for the boundary layer: Brief description and initial results. *J. Atmos. Ocean. Technol.* **5**:432-441.

Ghebrebrhan, O., 1990. Full decoding of truncated ranges for ST/MST radar applications. *IEEE Trans. Geosci. Remote Sens.* **28**:14-18.

Gossard, E. E., and R. G. Strauch, 1983. *Radar Observation of Clear Air and Clouds*. Elsevier Sci. Publ., Amsterdam, 280 pp.

Panofsky, H. A., and J. A. Dutton, 1984. *Atmospheric Turbulence. Models and Methods for Engineering Applications*. John Wiley & Sons, Inc., New York, 397 pp.

VanZandt, T. E., J. L. Green, K. S. Gate, and W. L. Clark, 1978. Vertical profiles of refractivity turbulence structure constant: Comparison of observations by the Sunset Radar with a new theoretical model. *Radio Sci.* **13**:819-829.

White, A. B., C. W. Fairall, and D. W. Thomson, 1991. Radar observations of humidity variability in and above the marine atmospheric boundary layer. *J. Atmos. Oceanic Technol.* **8**:639-658.

*U.S. GOVERNMENT PRINTING OFFICE:1994-573-013/00012